In-scene-based atmospheric correction of uncalibrated VISible-SWIR (VIS-SWIR) hyper- and multispectral imagery

L. S. Bernstein[a], S. M. Adler-Golden[a], R. L. Sundberg[*a] and A. J. Ratkowski[b]
[a]Spectral Sciences, Inc., 4 Fourth Avenue, Burlington, MA 01803-3304
[b]Air Force Research Laboratory, Hanscom AFB, MA 01731-3010

ABSTRACT

The QUAC (**Qu**ick **A**tmospheric **C**orrection) algorithm for in-scene-based atmospheric correction of VIS-SWIR (VISible-Short Wave InfraRed) Multi- and Hyperspectral Imagery (MSI and HSI) is reviewed and applied to radiometrically uncalibrated data. Quite good agreement was previously demonstrated for the retrieved pixel spectral reflectances between QUAC and the physics-based atmospheric correction code FLAASH (**F**ast **L**ine-of-sight **A**tmospheric **A**nalysis of **S**pectral **H**ypercubes) for a variety of HSI and MSI data cubes. In these code-to-code comparisons, all the data cubes were obtained with well-calibrated sensors. However, many sensors operate in an uncalibrated manner, precluding the use of physics-based codes to retrieve surface reflectance. The ability to retrieve absolute spectral reflectances from such sensors would significantly increase the utility of their data. We apply QUAC to calibrated and uncalibrated versions of the same Landsat MSI data cube, and demonstrate nearly identical retrieved spectral reflectances for the two data sets.

Keywords: hyperspectral, multispectral, atmospheric, correction, compensation

1. INTRODUCTION

If a spectral imaging sensor is radiometrically uncalibrated and/or poorly spectrally calibrated, first-principles atmospheric correction methods cannot be used to retrieve surface reflectances. The only recourse is to make assumptions about the spectral properties of the scene or about the materials within it. For example, assumptions may be made about the minimum spectral reflectance value (i.e., zero) and either a maximum value, such as unity for bright Lambertian surfaces or thick clouds[1], or assumed values for an identifiable reference spectrum. With this information one may derive a linear transformation, consisting of a spectral gain and offset, that only very approximately converts the data values to spectral reflectance. However, maximum reflectance values in real scenes can vary considerably, depending on the scene composition, pixel size, the presence of solar glints and the dynamic range of the sensor, which may saturate on bright materials. Similarly, the spectral reflectance of identified reference materials in a scene can often vary considerably and unpredictably from their library reference values depending on environmental conditions (aging, surface contamination, *etc.*) and illumination factors (bi-directional reflectance function effects, for example).

Previously, Bernstein *et al.*[2,3] showed that reflectance may be reasonably estimated from the statistical properties of diverse, non-vegetated pixels in an image selected by an automated endmember algorithm. In their original QUAC method, each offset-subtracted spectral channel is scaled by dividing by the endmember standard deviation. This procedure relies on the empirical observation that the reflectance standard deviation of a collection of diverse, non-vegetated materials tends to be spectrally flat.

The current paper reviews modifications to the QUAC method[4], yielding improved accuracy in the retrieved reflectances, in which an endmember *mean* spectrum rather than a *standard deviation* spectrum is used to define the scaling. We have observed that the mean of the endmember reflectance spectra, while not flat, tends to be quite consistent between reasonably complex land scenes and quite robust with respect to the number of endmembers selected and the details of the endmember selection method. In our typical test cases, mean reflectance errors in comparisons between the QUAC and FLAASH results[5-7] with this new method are found to be ~ ±15% (rms over all the spectral channels). In these code-to-code comparisons, all the data cubes were obtained with well-calibrated sensors. However, many sensors operate in an uncalibrated manner, precluding the use of physics-based codes to retrieve surface reflectance. The ability to retrieve absolute spectral reflectances from such sensors would significantly increase the

[*] rob@spectral.com; phone 1 781 273-4770; fax 1 781 270-1161; spectral.com

utility of their data. The applicability of QUAC to completely uncalibrated data is the focus of this work. We apply QUAC to calibrated and uncalibrated versions of the same Landsat MSI data cube. Starting with a well-calibrated Landsat data cube, we applied a linear transformation, consisting of a different gain and offset, to each spectral band to produce radiometrically uncalibrated data. QUAC was then applied to both the calibrated and uncalibrated data, and very close agreement (to within ~±2% rms over all the spectral channels) was found between the retrieved reflectance cubes. While we focus here on an MSI example, comparable results have been obtained for an AVIRIS HSI data cube.

2. OVERVIEW OF QUAC APPROACH

We present an overview of the QUAC method; a more detailed discussion can be found elsewhere.[4] Like the Empirical Line Method[8], QUAC assumes a linearized radiation transport equation in which data values are transformed to reflectance spectra via a spectral offset, or baseline, and a gain spectrum. In a scene of typical complexity and high to moderate (up to ~30 m) spatial resolution, it is very likely that near-zero reflectance values exist in each spectral channel, corresponding to the minimum data values in the scene (excluding corrupted or "bad" pixels). These minimum values, which typically occur with shadow, water bodies or dark green vegetation, determine the baseline.

Once the baseline is subtracted from the data, the remaining quantity to be determined is the gain spectrum. In QUAC, the gain spectrum is derived by comparing a statistic of the data with the same statistic applied to reflectance spectra. Spectral means, standard deviations or other statistics of the full scene are not suitable, as they are highly dependent on the relative abundances of the various types of materials and terrain. On the other hand, statistics derived from a spectrally diverse pixel subset avoid this problem, as long as a sufficient number and variety of such pixels are present.

In the current QUAC algorithm, the *relative gain spectrum* is taken as the ratio of a mean of reflectance endmembers to a mean of data endmembers. Reflectance means computed from endmembers of a diverse, artificial reference "scene" are shown in Figure 1. This reference scene is a collection of 195 material reflectance spectra with green vegetation excluded. The spectra consist of the Johns Hopkins University libraries[9] of soils, terrestrial coarse-ground minerals, and manmade materials, augmented by dry vegetation spectra compiled by Elvidge[10]. The spectra were resampled to AVIRIS sensor wavelengths, and endmembers were selected using the automated SMACC (Sequential Maximum Angle Convex Cone) method[11] employing positivity and sum-to-unity constraints. To save computation time, and to enable operation with multispectral sensors having as few as four spectral channels, subsets of between four and six "window region" spectral channels were used in the endmember selection. The number of spectral channels used does not limit the number of endmembers that SMACC can retrieve.

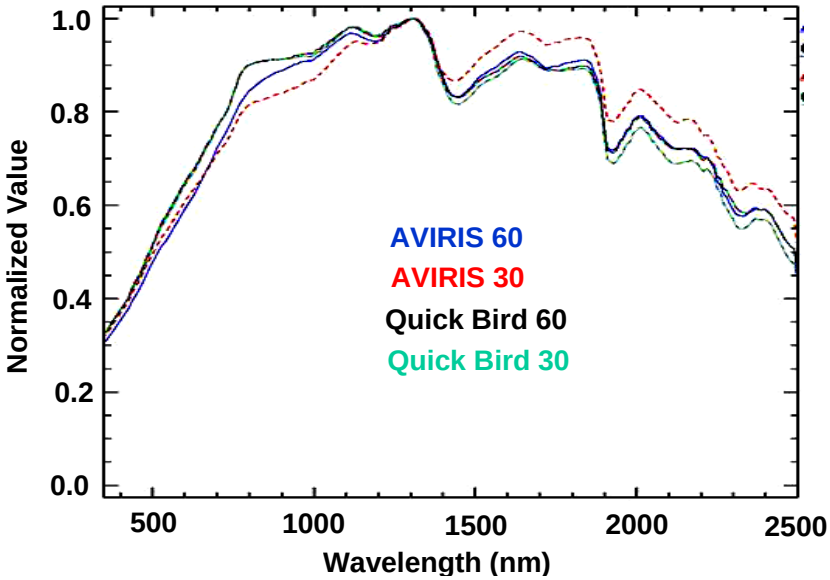

Fig. 1. Normalized mean spectra of endmembers selected from a 195-material library. Different numbers of endmembers (30 or 60) and different wavelength channels were used for selection. AVIRIS channels are at 500, 863, 1027, 1246, 1612 and 2150 nm; QuickBird channels are located at 485, 560, 660 and 830 nm.

As shown in Figure 1, the mean of the endmember reflectance spectra is found to be remarkably insensitive to the number and location of the spectral channels and the number of selected endmembers over fairly wide ranges, particularly if the curves are normalized to the same magnitude. With around 20 endmembers or less, statistical fluctuations appear, and around 80 endmembers or more, the material abundances in the scene become important. If a major material type, such as dry vegetation, is absent from the scene, the mean is more significantly affected. The similarity of the curves in Figure 1 suggests that, in scenes containing all material types, a "universal" mean reflectance spectrum can serve as a reasonable reference for the gain computation. However, to account for subtle dependences of the mean reflectance spectrum on the specific sensor channels and to allow customization of the reference scene, the current QUAC algorithm calculates this reference spectrum on the fly as part of the data analysis. The default reference "scene" is the 195-member reflectance library described above.

Prior to finding the data endmembers, the data are normalized to relative apparent reflectance by dividing by the solar function. This normalization step improves the correspondence between the data endmembers and reference scene (reflectance) endmembers by providing a more uniform weighting of the data at different wavelengths.

The absolute magnitude of the relative gain spectrum, which determines the absolute magnitude of the reflectances, can be estimated by several methods. If the sensor has an accurate radiometric calibration at an infrared "window" wavelength such as ~2.2 μm, where atmospheric transmittance is typically ~90% or greater, the magnitude can be set to match the reflectance to the apparent reflectance. This is readily calculated from the solar irradiance function and the presumably known solar elevation angle. Otherwise, the magnitude may be estimated by fixing the reflectance value of an identifiable surface material, such as vegetation, at one (or more) wavelengths. In the present algorithm, vegetation pixels with an NDVI of greater than 0.7 are selected and their ~0.83 μm reflectance average value set to 0.4. If minimal vegetation is present, the absolute gain spectrum is based on the reference endmember average.

There is no rigorous theoretical underpinning for QUAC. However, we can provide a qualitative explanation for why it works. The scene-derived endmembers tend to uniformly sample a wide range of material reflectance values (i.e., dark to bright) for each spectral channel. The endmember-averaged material reflectance spectrum is insensitive to the scene specifics, as long as the scene contains enough diverse pixel spectra to span the reflectance range for each spectral channel. The shape of the endmember reference reflectance spectrum is controlled by stronger material absorption features at either end of the spectrum, IR absorption bands at the red end and electronic absorption bands at the blue end.

Example comparisons of QUAC to FLAASH for well-calibrated HSI and MSI data sets are presented in Figure 2. In the following section, we investigate the level of degradation of the QUAC results when it is applied to uncalibrated data.

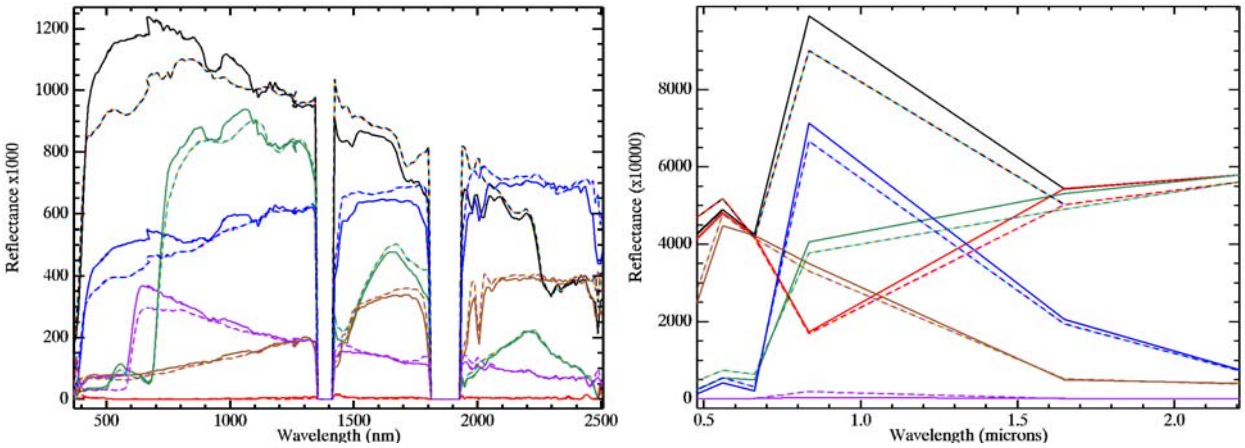

Fig. 2. Comparisons of QUAC (dashed lines) and FLAASH (solid lines) reflectance spectra for the HSI AVIRIS (top) and MSI Landsat7 (bottom) data sets.

3. APPLICATION OF QUAC TO UNCALIBRATED DATA

This study was performed with Landsat7 data of the area around Davis, CA, which is rendered as an RGB composite picture in Figure 3. The data, in six bands from 450-2500 nm at a GSD (Ground Sample Distance) of ~30 m, were obtained with the ETM+ sensor. Example data spectral curves, spanning the full intensity range of the scene, are presented in Figure 4. The lower spectral curve corresponds to the darkest material, which for this scene is defined by the water body in the upper right hand corner of the image. The upper spectral curve corresponds to the brightest feature for each channel, which likely originates from the bright and white man-made structures. An uncalibrated version of this data was simulated by applying very different gains and offsets to each spectral channel. The result is shown in Figure 5. By comparison to Figure 4, it is seen that the uncalibrated data bears no obvious resemblance to the calibrated data. We also deleted the blue Landsat channel centered on ~450 nm from our simulated uncalibrated sensor data, as many multispectral sensors do not contain channels below ~500 nm.

An unforeseen consequence of the particular transform used to produce the uncalibrated data is the steep increase in intensity for all the pixels in going from ~650 to 800 nm. This resulted in a situation where every pixel appeared to have a strong red edge and was therefore flagged by QUAC as a vegetation pixel. Vegetation pixels are not considered for endmember selection in QUAC. In order to remedy this situation, a "correction" transformation was sought that enabled the vegetation spectrum to be differentiated from non-vegetation spectra. The approach adopted was to define this linear transform by an offset corresponding to the darkest value for each channel and a gain corresponding to the inverse of the brightest value for each channel. This transform results in a very approximate correction of the data to spectral reflectance, one that is much less accurate than the QUAC result. However, as seen in Figure 6, it is sufficient to separate the vegetation from the non-vegetation spectra. After application of this vegetation-pixel identification method, the standard QUAC algorithm was then applied to the uncalibrated data. The resulting reflectance spectra are compared to those obtained from the calibrated data in Figure 7. The differences are minor, and are attributed to differences in the endmembers selected for each data set.

Fig. 3. RGB composite of Landsat7 data in the vicinity of Davis, CA. The image is ~ 65 km wide.

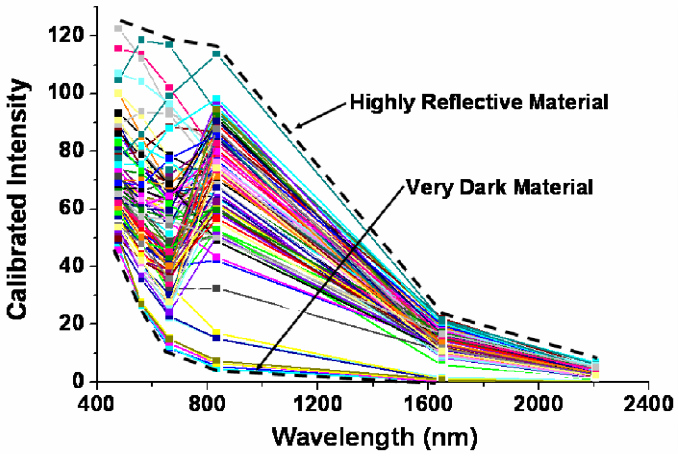

Fig. 4. Sample spectra for the calibrated Landsat7 data indicating the upper and lower spectral envelopes.

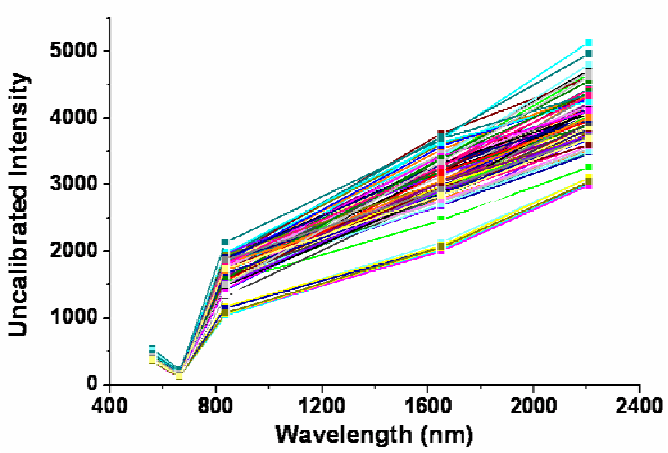

Fig. 5. Same sample spectra as in Figure 4 but after the application of a linear transformation to simulate uncalibrated Landsat7 data.

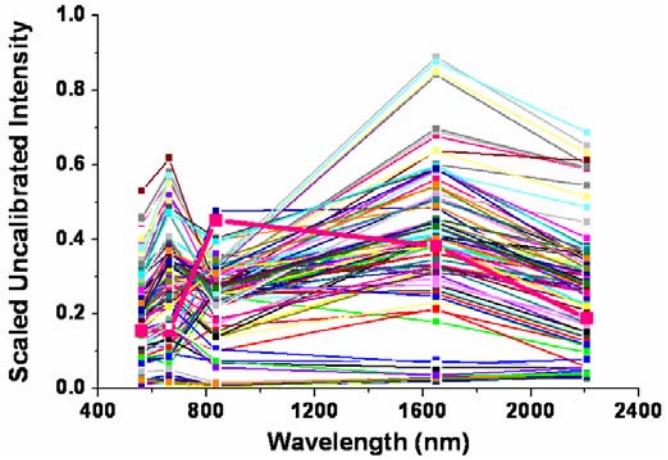

Fig. 6. Same sample spectra as in Figure 5 but after application of a linear transformation to enable identification of vegetation spectra via the strong red edge feature around ~750 nm. An example vegetation spectrum is highlighted by the thick pink curve.

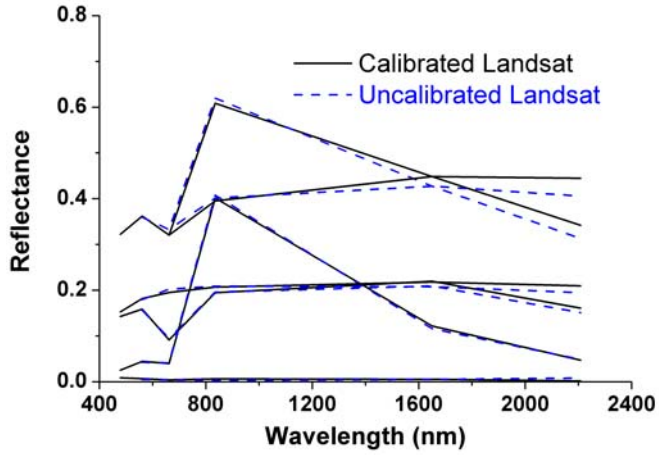

Fig. 7. Comparison of QUAC-retrieved reflectances for the calibrated and uncalibrated Landsat7 data.

4. CONCLUDING REMARKS

Because QUAC is based on a linear transformation derived solely from the data itself, it is essentially invariant to any additional and arbitrary linear transform applied to the data. Therefore, it is not surprising that QUAC performs comparably well on calibrated and uncalibrated data. Nevertheless, it proved a worthwhile exercise to demonstrate this point, as it revealed other problems with the application of QUAC to uncalibrated data, namely the issue of vegetation removal. While this study focused on radiometrically uncalibrated data, QUAC will also work well with radiometrically calibrated and uncalibrated data with poor spectral calibration. However, some approximate knowledge of the correspondence between channel number and wavelength is required in order to determine which channels are to be used for vegetation removal, as well as to allow a meaningful interpretation of the results.

We anticipate implementing a number of upgrades to QUAC over the next year, including:

- Improving the absolute accuracy of the retrieved reflectances by comparison of the endmembers to a reference material library,
- Applying QUAC to non-ideal viewing conditions, such as under complete cloud cover and to cloud-shadowed regions, and
- Applying QUAC to sensors that do not contain visible channels, which requires implementation of a new vegetation removal algorithm based on the NIR-SWIR (~0.9-2.5 μm) spectral domain.

5. ACKNOWLEDGMENTS

Spectral Sciences, Inc. (SSI) efforts were funded in part through the AFRL Phase II SBIR project FA8718-05-C-0008 and in part as an SSI Internal Research and Development project. We thank M. Hoke and G. Felde of the Air Force Research Laboratory for technical discussions. We also appreciate technical discussions with P. Villeneuve, A. Stocker and A. Oshagan of the Space Computer Corporation, and S. Reuman of the Goodrich Corporation.

REFERENCES

[1] Mustard, J.F. and Prell, W., "Diverse spectral properties in a temperate estuary: First results from Narragansett Bay, Rhode Island," Summaries of the 7th JPL Airborne Earth Science Workshop, Vol. 1, pp. 97-21, (1998).

[2] Bernstein, L.S., Adler-Golden, S.M., Sundberg, R.L., Levine, R.Y., Perkins, T.C., Berk, A., Ratkowski, A.J. and Hoke, M.L., "A New Method for Atmospheric Correction and Aerosol Optical Property Retrieval for Vis-SWIR Multi- and Hyperspectral Imaging Sensors: QUAC (QUick Atmospheric Correction)," Proc. 13th JPL Airborne Earth Science Workshop, (April 2004) (available from www.aviris.jpl.nasa. gov).

[3] Bernstein, L.S., Adler-Golden, S.M., Sundberg, R.L., Levine, R.Y., Perkins, T.C. and Berk, A., "Validation of the QUick Atmospheric Correction (QUAC) algorithm for VNIR-SWIR multi- and hyperspectral imagery," SPIE,Proceeding Algorithms and Technologies for Multispectral, Hyperspectral and Ultraspectral Imagery XI, Sylvia S. Shen and Paul E. Lewis, Eds., Vol. 5806, pp. 668-678, (June 2005).

[4] Bernstein, L.S., Adler-Golden, S.M., Sundberg, R.L. and Ratkowski, A.J., "Improved reflectance retrieval from hyper- and multispectral imagery without prior scene or sensor information," Proc. SPIE Remote Sensing of Clouds and the Atmosphere XI, Vol. 6362, pp. 63622P, (October 2006).

[5] Adler-Golden, S.M., Matthew, M.W., Bernstein, L.S., Levine, R.Y., Berk, A., Richtsmeier, S.C., Acharya, P.K., Anderson, G.P., Felde, G., Gardner, J., Hoke, M., Jeong, L.S., Pukall, B., Mello, J., Ratkowski, A. and Burke, H.-H., "Atmospheric Correction for Short-wave Spectral Imagery based on MODTRAN4," SPIE Proceeding, Imaging Spectrometry V, Vol. 3753, pp. 61-69, (October 1999).

[6] Matthew, M.W., Adler-Golden, S.M., Berk, A., Felde, G., Anderson, G.P., Gorodetzky, D., Paswaters, S. and Shippert, M., "Atmospheric Correction of Spectral Imagery: Evaluation of the FLAASH Algorithm with AVIRIS Data," SPIE Proceeding, Algorithms and Technologies for Multispectral, Hyperspectral, and Ultraspectral Imagery IX, Vol. 5093, pp. 474-482 (September 2003).

[7] Matthew, M.W., Adler-Golden, S.M., Berk, A., Richtsmeier, S.C., Levine, R.Y., Bernstein, L.S., Acharya, P.K., Anderson, G.P., Felde, G.W., Hoke, M.P., Ratkowski, A., Burke, H.-H., Kaiser, R.D. and Miller, D.P., "Status of

Atmospheric Correction Using a MODTRAN4-based Algorithm," SPIE Proceeding, Algorithms for Multispectral, Hyperspectral, and Ultraspectral Imagery VI, Vol. 4049, pp. 199-207 (2000).

[8] Roberts, D.A., Yamaguchi, Y., and Lyon, R.J.P., "Calibration of Airborne Imaging Spectrometer data to percent reflectance using field spectral measurements," 19th International Symposium on Remote Sensing of Environment, Ann Arbor, MI, pp. 679-688, (October 1985).

[9] Johns Hopkins University spectral library, available from http://speclib.jpl.nasa.gov/ (2006).

[10] Elvidge, C.D., "Visible and infrared reflectance characteristics of dry plant materials," Int. J. of Remote Sensing, vol. 11, no. 10, p. 1775 – 1795 (1990).

[11] Gruninger, J., Lee, J. and Sundberg, R.L., "The Application of Convex Cone Analysis to Hyperspectral and Multispectral Scenes," SPIE Proceedings Image and Signal Processing for Remote Sensing VIII, Vol. 4888, pp. 188-198, (March 2003).